Capillary Effect of Hydrophobic Polyester Fiber Bundles with Noncircular Cross Section

Y. Zhang,[1,2] **H. P. Wang,**[2] **Y. H. Chen**[1]

[1]Textile College, Dong Hua University, Shanghai 200051, People's Republic of China
[2]State Key Laboratory for Modification of Chemical Fibers and Polymer Materials, Dong Hua University, Shanghai 200051, People's Republic of China

ABSTRACT: Moisture transport in fiber assembly is one of the critical factors affecting physiological comfort. It is useful to model bundle structure for understanding capillary flow in complex geometries representative of the void spaces formed between fibers. A new mathematical model MFB has been used to simulate alignment representative of void spaces formed between fibers in noncircular cross section fiber bundles. Fiber morphological character and their random packing pattern are emphasized to discuss the mechanism of capillary flow in fiber assembly in this work. Capillary equivalent radius distribution, flux of saturated fiber bundle, capillary generating ability, and wicking velocity are computed to predict which kind of shape is predominant for hydrophobic polyester fiber wicking. Vertical wicking model of polyester filaments bundle predicts that as the nonroundness of filaments increase, the maximum liquid height, flux of saturated bundle, and capillary forming ability will increase, while instantaneous wicking velocity increases not stably. Concave polygon shape of fiber bundle has much more small capillary tubes than convex shape of fiber bundle. © 2006 Wiley Periodicals, Inc. J Appl Polym Sci 102: 1405–1412, 2006

Key words: cross-sectional shape; hydrophobic polyester fiber; wicking; capillary; fiber bundle

INTRODUCTION

Liquid transport in textile medium is one of the critical factors affecting fabric functional application. Fabric that can transfer moisture away or keep liquid flowing rapidly through affords quick drying and physiological comfort for wearers. Liquid is transported by capillary action through fabric pores formed between fibers in textile assembly. Momentum of penetration and transportation of liquid in fiber bundle is through capillary force caused by interface tension, which is affected by fiber surface area. So fiber configuration and fiber arrangement in textile influence capillary action greatly.[1,2] Mathematical modeling of surface-tension-driven flowing structure in fiber assembly provides an efficient way to understand geometric figuration and material parameters for investigating liquid transport in fibrous media.

According to geometry size and formation way, fabric interplace can be classified into yarn-space (interplace between fabric stitch), fiber-space (interplace inside of yarn) as well as micro-space or amorphous region inside of fiber. Fiber-space and micro-space are very important for liquid flowing in long range. However, for some materials, fiber cannot absorb liquid into fiber body considerably. So fiber-space that is affected by fiber alignment plays an important role for hydrophobic polyester fiber wicking.[3]

Capillary flow in textile assembly has been extensively studied.[1,4–7] Early in 1920, Washburn has already reviewed dynamics of capillary flow.[8]. He confirmed that the equivalent radius of capillary tube is one of the most important parameters for liquid flowing in capillary assembly.

To understand the role of geometric and material parameters in yarn package, many mathematical models have long been used to interpret results of wicking.[9–13] In Dilip's model of capillary flow, he focused on the effect of geometric and material parameters on moisture transport.[2] He discussed relationship between fiber number and liquid wicking height and velocity by a uniform arrayed fiber bundle model. More recently, Lukas et al. also have done much notable work about liquid wetting and ascending along fiber bundle by 3D Ising computational model.[1,14,15] Lukas and Ning showed us a model of bundle cross section based upon physical fluid flow dynamic and 3D Ising model, which is found on minimum conversation of energy.[1] However, cylindrical capillary ge-

ometry used in these models makes it difficult to understand the role of fiber shape and random arrangement on wicking in bundles.

Enlarging the specific surface-area of fibers by changing fiber shape is a reasonable way to improve capillary force of hydrophobic polyester fiber bundle and to meliorate the wicking of polyester fabric.[16,17] As Lukas' remarks about the effect of individual fiber morphology, proper shape of fiber cross section will effectively improve the liquid transport ability.[14] Marcus' work[11] shows that cross section shape affects the capillary action markedly, which confirmed Lukas's remarks mentioned before. Polymeric fiber with four tunnels (Coolmax) made by Dupont has been also proved with excellent capillary effect compared to normal circular cross section fiber practically.

Therefore, we aim to shape fiber cross section individually to increase specific surface-area of fibers based on surface-driven-flow mechanism and to compare alignments of shaped fiber by four parameters for estimating which kind of shape is better for wicking array.

Hearle et al.[7] discussed the yarn idealized packing earlier in the 20th century.[7] Lukas adopt the open packing of circular fibers from Hearle's model in his work about wetting of a fiber bundle in fibrous structure. But their packing models are too idealized to describe the real position of fiber in bundles. The computational simulative model we used in this paper to predict the capillary flow in fiber bundle is a stochastic approach to pattern the real position of fibers in bundle. Capillary equivalent radius distribution, flux of saturated fiber bundle, capillary generating ability, and wicking velocity are computed to predict which kind of shape is predominant for hydrophobic polyester fiber wicking.

MODEL ASSUMPTION

Precondition of capillary action is additive pressure not less than liquid gravity in capillary tube. The corresponding expressions are as in eq. (1).

$$\frac{2\sigma \cos\theta}{r}\pi r^2 - \pi r^2 h\rho g > 0 \qquad (1)$$

where h, g, and ρ are the capillary liquid height (m), acceleration of gravity (m/s^2), and liquid density (kg/m^3), respectively. And r, θ, and σ are equivalent radius of capillary (m), liquid–gas contact angle, and liquid–gas interfacial tension (N/m), [20°C, water = 0.0725 (N/m)].

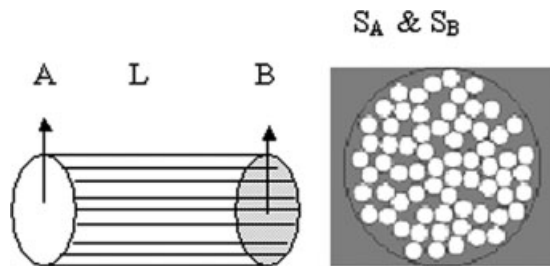Based on eq. (1), capillary liquid height has to satisfy the following condition:

Figure 1 Model of fiber bundle.

$$h \leq \frac{2\sigma \cos\theta}{r\rho g} \qquad (2)$$

Obviously if fiber and liquid properties are invariable, capillary height will be higher when the equivalent radius is smaller.

Under the conditions where inertia is not important,[18] Reed and Wilson solved the force balance to derive the following expression for the time t required by the liquid to reach a height h:

$$t = \frac{8\eta}{\rho g r^2}\left[(h_\infty + h_0)\ln\left(\frac{h_\infty}{h_\infty - h}\right) - h\right] \qquad (3)$$

where h_∞, h_0 mean maximum wicking height and initial height, respectively. Distance of liquid motion in every unit time is inversely proportion to square of capillary equivalent radius. According to the Reynolds' criterion, equivalent radius is also proportion to the wicking rate inversely. Therefore, equivalent radius is very critical for investigating liquid transport in capillary bundles. So capillary equivalent radius is one of the important parameters for modeling. A shaped fiber bundle model is prepared to simulate the real stochastic position of hydrophobic polyester fiber bundle.

This model has following suppositions. (a) Filaments with shaped cross section are paralleled to each other and packed stochastically. (b) Every void space between fibers is capillary tube characterized by equivalent radius. (c) A dot along the axis of bundle is A that lies in a cross section plane of bundle vertical to the axis. Similarly another dot B_{A+L} in the plane of S_B has a distance L with A along the bundle axis. (d) Fiber is rigid monomer, which can keep its configuration invariable even on the pressure. (e) In every cross section of bundle like S_A or S_B, fibers are packed randomly and irregularly, which is parabolic with the real position.

This filament bundle model is named as "Model of Fiber Bundle (MFB)," which is shown in Figure 1. MFB can be taken as a micro-unit along bundle and fibers are paralleled with each other in the unit. MFB is available to any yarn structure as long as L is small

enough. The fiber shape (v) is a variable of MFB cross section.

$$U = \phi(\nu) \tag{4}$$

U is the simulated alignment pattern of MFB, and v is fiber shape, which can be round, triangle, square, cross–shaped, i.e., v can be designed and amended as required by engineering manufacturing problem. Figure 3 illustrates three shape designs of the single fiber.

ϕ is a random function based on the real physical position of fibers in bundle. The work about fiber arraying in bundle drew more attention to the evaluation of idealized alignment of fibers in bundles, such as opening array or closed array. Actually single fibers are arrayed in bundles stochastically.[7] The function (ϕ) is defined as a method of how fibers are forming in the bundle. When the cross section pattern of bundle is created, fibers move to the axes of bundle from any angle on the circle of bundle's cross section circumcircle randomly one by one. The bundle body circle is divided into 720 parts of angle, which means the starting point may stay at any circumferential 0.5° dot. During the process of moving towards the axes of bundle, the fiber will not stop until it meets another located fiber. Then the moving fiber will sway around to look for more appropriate location nearer to the center. Since fiber is assumed to be a rigid unit, there is no deformation and no cross-sectional superposition for fibers occurring caused by moving impact.

MFB MODELING

To realize the alignment pattern of fibers in bundle stochastically similar to real packing way, a mathematical computer program is designed to simulate the real position. In creating cross section of bundle computer program named Shape-Generator, Visual C++ has been used to define the random function ϕ.

Principium of SG's data generation is based on pixels calculation. SG search for pixels on the objective area and recalculate them into the effective physical value.

$$S_c = A_{(x)}\alpha \tag{5}$$

where S_c is objective area, $A_{(x)}$ is the number of pixels in this area, α presents the actual physical quantity for one pixel, like 7.42×10^{-4} mm/pixel. α as the geometric size of bundle is invariable. SG will transform pixel number into physical data for the objective area automatically.

Magnitude of SG is defined based on the real size of fiber and bundle. Magnitude of general polyester filament's radius is about 10 to 10^{-2} mm, namely 1–10 μm. For example, poly(trimethylene terephthalate) filament tow (110 dtex/48 f) with the density of 1.33
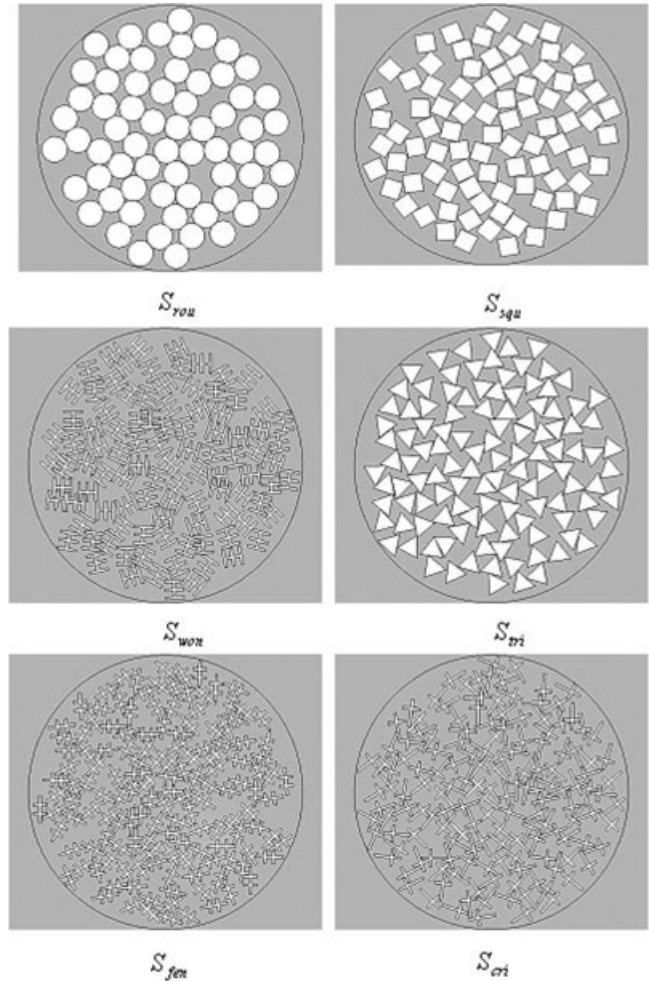

Figure 2 Bundle cross sections with different shape fiber.

mg/mm^3 has single filament cross-sectional area of 1.729×10^{-4} mm^2. If the cross section shape of filament is round, radius will be 7.42×10^{-3} mm. In the conceive of creating cross section of bundle, individual fiber circum-circular radius is assumed to be 1.0×10^{-2} mm. Fiber radius verses bundle radius is 1:10. Appliance of SG in this paper has α of 7.42×10^{-4} mm/pixel.

Since the geometric size of interplace forming between fibers is critical for liquid flow in fiber bundle, it is necessary to acquire the parameters of capillary space. SG counts the pixel number in one cross section of capillary tube and transforms it into the value of super area. The area is assumed to be round shape, and so the equivalent radius r of capillary space will be computed mathematically.

The perimeter of capillary C is not an equivalent value, but a real length of erose capillary cross section that is also transformed by pixel counting.

Six machinable shapes in Figure 2 are demonstrated to compare their simulative system parameters and corresponding relationship with wicking effect. Table I states the fiber code and shape design.

TABLE I
Code Number of Filaments

Serial number	Fiber code	Shape of cross-section
1	S_{rou}	Round
2	S_{squ}	Square
3	S_{won}	**H**
4	S_{tri}	Triangle
5	S_{fen}	**+**
6	S_{cri}	Crisscross

Figure 4   Distribution of equivalent radius.

S_{rou} has a circular fiber cross section; S_{squ} has a square one, and S_{tri} has equiangular triangle one. S_{won} has three parallel strips distributed equably, which are perpendicular to another strip in same length. Width of strip can be varied or adjusted at certain extent, which is set to be 1–7 of strip length. In Figure 3, it shows the pattern design of S_{won}.

Fiber in S_{fen} is double regular crisscross superposed together partially, which has the same width size as S_{won}. In S_{cri} a/b is 2, which is also shown in Figure 3.

To get more steady and reliable simulating data, a computational method is used to establish the frequency of simulation.

$$\omega = \frac{R_{N_i} - R_{N_{i-m}}}{R_{N_i}} \times 100\% \quad m = (1,2,3,4,5) \quad (6)$$

where ω means precision of modeling times, R is average equivalent radius of capillary for a bundle, N_i and N_{i-m} are time of modeling. After SG is run for certain times, equivalent radius values will remain stable comparatively. ω is the coefficient revealing extent of stabilization. Here we define that ω is not higher than 0.5%, which is converted to not less than 20 times.

RESULTS AND DISCUSSION

Equivalent radius values and their distribution in 0.01–6 μm simulated by SG are shown in Figure 4. Capillary tubes frequencies and their distributions are shown in Figure 5. Equivalent radius values of capil-
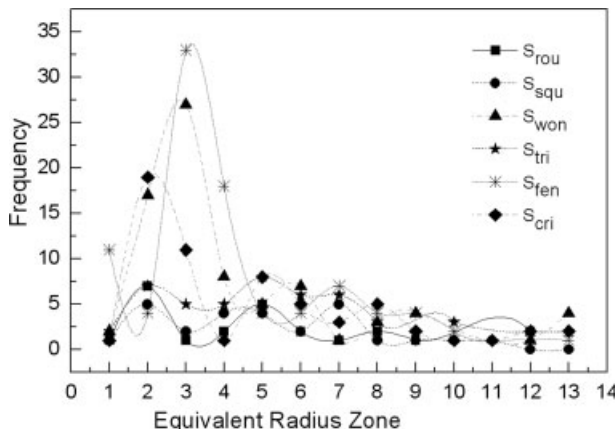
lary tubes are divided into 13 sub-domains (Table II). The radius smaller than 0.01 μm is defined as microcapillary and the one bigger than 6 μm as macrocapillary here. Actually, there is an effective range for interspace formed between fibers to be named capillary tube with wicking effect, which is defined to $r_{min} < r < r_{max}$. Since interspaces of polyester fiber and macro-space formed between yarns affect little for liquid transportation in fiber bundle,[8] we will concentrate to investigate medium space, namely intermediate capillary tubes.

To evaluate the wicking action of fiber bundles, we compute the wicking height, capillary frequency, saturated liquid quantity flux, and wicking rate theoretically by mathematical simulation.

Distribution of capillary equivalent radius of fiber bundles

Figure 4 shows that S_{won}, S_{fen}, and S_{cri} have a convergence in the low radius value range compared to the other three. In range 3rd of $(0.100-0.150) \times 10$ μm, S_{fen} has 33 capillaries, S_{won} has 27, and S_{cri} has 19. Noncircular fibers present uptrend in small capillary tubes. Furthermore, these three fibers all reach their frequency peak in range 3. The other three fibers distribute equably in $(0.001-0.500) \times 10 \mu$m, and frequencies are 5–10 roughly. However, not all noncircular
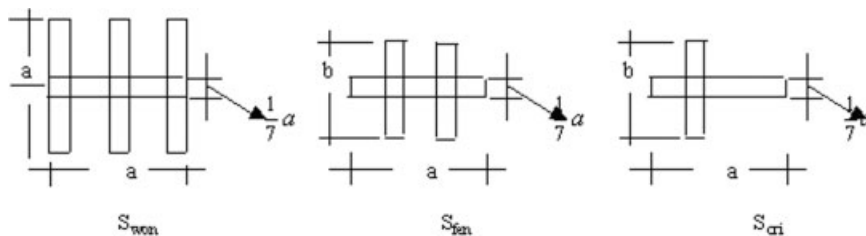

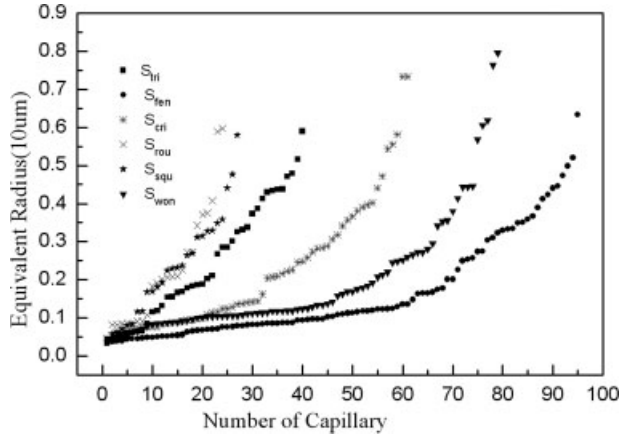**Figure 3**   Shape designs of S_{won}, S_{fen}, and S_{cri}.

Figure 5 Equivalent radius value distributions.

fibers present uptrend in small capillary tubes. It can be found that only concave polygon fibers do have more small capillary tubes. From eqs. (1) and (2), we know that same count yarn will have more capillary tubes with small radius, and liquid creeping height of capillary will be higher. Therefore, we acquire the sequence of wicking height ability shown as

$$S_{fen} > S_{won} > S_{cri} > S_{tri} > S_{squ} > S_{rou}.$$

Figure 5 reveals the relationship between capillary equivalent radius and its frequency. Capillary frequencies of S_{won}, S_{fen}, and S_{cri} are much more than other three contrastively and they converge on small radius values. Concave polygon fiber bundles have macro-space possibly, but most of capillary spaces are very small. Meanwhile, the other three capillary numbers are all below 40, which mean they cannot generate more capillary space. So concave polygon fiber bundle has more small capillary tubes than convex shape of fiber bundle.

TABLE II
Number List of Radius Range

Serial number	Equivalent radius of capillary (10^{-6} m)
1	0.01–0.50
2	0.50–1.00
3	1.00–1.50
4	1.50–2.00
5	2.00–2.50
6	2.50–3.00
7	3.00–3.50
8	3.50–4.00
9	4.00–4.50
10	4.50–5.00
11	5.00–5.50
12	5.50–6.00
13	6.00

TABLE III
Flux of Saturated Fiber Bundles

Fiber code	
S_{rou}	5.395083
S_{squ}	6.277257
S_{won}	15.5346
S_{tri}	9.754418
S_{fen}	15.72553
S_{cri}	13.58044

Flux of saturated fiber bundle

Liquid quantity in bundle is also an important physical parameter for estimating wicking. We take the flux of saturated fiber bundle as one comparison operator. Capillary maximum height can be calculated from eq. (2), which is shown as eq. (7).

$$h = \frac{2\sigma \cos\theta}{r\rho g} \tag{7}$$

Neglecting curve effect at the end of liquid column, the liquid volume in capillary tube is

$$Q = \pi r_{(x)} e x 2h = \pi r_{(x)}^2 \frac{2\sigma \cos\theta}{r_{(x)}\rho g} \tag{8}$$

So the flux in bundle will be

$$\sum_{x=1}^{n} Q_x = \sum_{x=1}^{n} \pi r_{(x)}^2 h_{(x)} = \sum_{x=1}^{n} \pi r_{(x)}^2 \frac{2\sigma \cos\theta}{r_{(x)}\rho g}$$

$$= \sum_{x=1}^{n} \frac{2\pi\sigma \cos\theta}{\rho g} \times r_{(x)} \tag{9}$$

Equation (9) shows that the pivotal ingredient of liquid flux relies on the accumulative total value of equivalent radius. Table III presents flux values of shaped fiber bundles.

Evidently, sequence of saturated liquid quantities is also $S_{fen} > S_{won} > S_{cri} > S_{tri} > S_{squ} > S_{rou}.$

Fiber and capillary frequency

Same count yarn with different cross-sectional shape will have dissimilar capillary space. Figure 6 shows the relationship between fiber and capillary frequency. Apparently, individual type of fiber has its correspondence principle.

Based on Figure 6, Table IV presents a quantificational comparison between six bundles. Capillary frequencies of S_{rou}, S_{squ}, and S_{tri} are around 30, but the other three are much bigger as about 80. Therefore, it is confirmed that concave polygon fiber bundle has
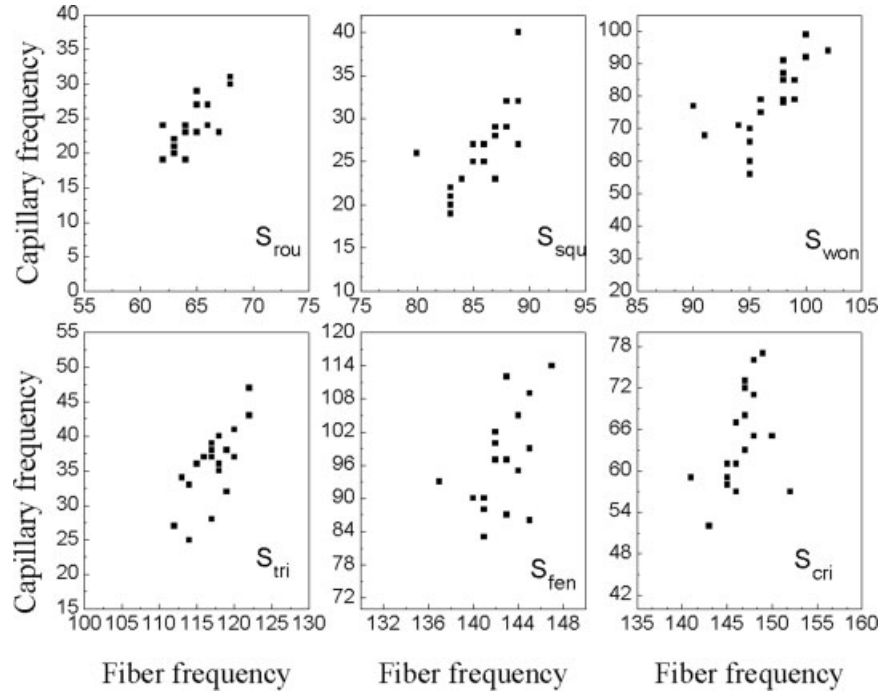
Figure 6 Frequency relationships between fiber and capillary.

much more capillary tubes than convex shape of fiber bundle.

Same count yarn with different fiber shape has dissimilar capillary space, what about the capillary space of shaped fibers with same fiber number? Figure 7 illustrates the capillary forming ability for six fibers. K is the coefficient, which is acquired by average capillary frequency dividing average fiber frequency in Figure 6. So the sequence of capillary forming ability is $S_{won} > S_{fen} > S_{cri} > S_{tri} > S_{rou} > S_{squ}$.

Wicking velocity

As penetrated velocity influence instantaneous liquid transportation when fiber bundle contact with liquid initially, we take the initial instantaneous wicking velocity as investigated object. Reed and Wilson's liquid arising in capillary theory[18] can be written as follow:

$$\left.\frac{\partial h}{\partial t}\right|_{t=0} = \frac{\rho g r^2 h_\infty}{8\eta h_0} \tag{10}$$

where t is wicking time, ρ is the density of liquid, η is the viscosity of liquid, and g is the acceleration of gravity.

$$h_\infty = \frac{CT \cos\theta}{A\rho g} \tag{11}$$

where h_∞ is the maximum height of capillary liquid, C is the perimeter of capillary, A is the area of capillary, and θ is the contact angle between liquid and fiber. Reed and Wilson's equations of dynamic flow in cap-

TABLE IV
Frequency Numerical Relationships Between Fiber and Capillary

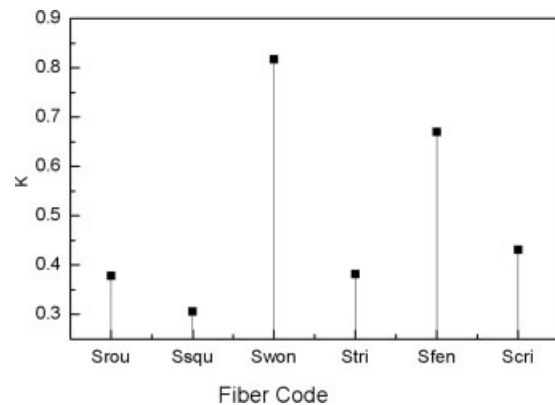| Fiber number	Fiber frequency	Capillary frequency
S_{rou}	60–80	20–30
S_{squ}	80–90	20–30
S_{won}	90–100	60–90
S_{tri}	100–120	25–40
S_{fen}	140–145	80–120
S_{cri}	140–150	50–80

Figure 7 Capillary forming ability for fibers.

TABLE V
Original Parameters of Capillary Pore
for Six Individual Shapes

Shape code	A (10^{-11} m)	C (10^{-5} m)	r (10^{-6} m)	$\left.\frac{\partial h}{\partial t}\right|_{t=0}$ (10^{-3} m/s)
S_{rou}	1.602	1.8085	2.258	2.5779
S_{tri}	1.392	1.6383	2.105	2.3472
S_{cri}	1.542	1.117	2.215	1.5993
S_{squ}	1.57	1.8191	2.235	2.6045
S_{won}	1.521	1.6489	2.2	2.3611
S_{fen}	1.606	2.0638	2.261	2.9562

illary provide the fundamental physical computation method for instantaneous wicking velocity.

We selected six individual capillary tubes with similar value of equivalent radius from six simulated bundle models to compare their penetrated wicking velocity. The original parameters of capillary tubes are shown in Table V.

To compare the wicking velocity of individual shape fibers expediently, equivalent radii of the other five capillaries are assumed to the same value as the one of round fiber. All the capillaries will have same equivalent radius and individual capillary morphology forming between six shapes of fibers separately. So the final result will reveal the effect of fiber morphology on the wicking velocity independently. The new data is acquired by eqs. (12) and (13).

$$\frac{\beta r_1}{\beta r_2} = \frac{C_1}{C_2} \tag{12}$$

$$\frac{\pi r_1^2}{\pi r_2^2} = \frac{A_1}{A_2} \tag{13}$$

β is the coefficient of capillary equivalent radius r and perimeter C. Since C_1 and C_2 have the same capillary morphology but different geometric size, β is invariable. C_1, A_1 and C_2, A_2 means original and amended parameters separately.

TABLE VI
Amendatory Parameters of Capillary Pore
for Six Individual Shapes

Shape code	A (10^{-11} m)	C (10^{-5} m)	r (10^{-6} m)	$\left.\frac{\partial h}{\partial t}\right|_{t=0}$ (10^{-3} m/s)
S_{rou}	1.602	1.8085	2.258	2.5779
S_{tri}	1.6017	1.7574	2.258	2.5174
S_{cri}	1.6025	1.1387	2.258	1.6303
S_{squ}	1.6025	1.8378	2.258	2.6312
S_{won}	1.6023	1.6924	2.258	2.4234
S_{fen}	1.6017	2.0611	2.258	17.2769

TABLE VII
Sequences of Physical Parameters
for Shaped Fiber Bundle

Physical parameters	Sequence
Liquid height	$S_{fen} > S_{won} > S_{cri} > S_{tri} > S_{squ} > S_{rou}$
Flux of fiber bundle	$S_{fen} > S_{won} > S_{cri} > S_{tri} > S_{squ} > S_{rou}$
Capillary number	$S_{won} > S_{fen} > S_{cri} > S_{tri} > S_{rou} > S_{squ}$
Wicking rate	$S_{fen} > S_{squ} > S_{rou} > S_{tri} > S_{won} > S_{cri}$

Amended data are presented in Table VI. Obviously, S_{fen} has the biggest instantaneous wicking velocity. Here $h_0 = 0.001$ m, $\theta = 60°$, $T = 7.2 \times 10^{-3}$ N/m, $\rho = 1000$ kg/m, $\eta = 1 \times 10^{-3}$ Pa, $g = 9.82$ m/s^2.[2]

Instantaneous penetration velocities of six type fibers have the following sequence:

$S_{fen} > S_{squ} > S_{rou} > S_{tri} > S_{won} > S_{cri}$.

The shape of crisscross is not good for increasing instantaneous wicking rate but it can have higher wicking height and more liquid flux for the reason of small capillary tubes.

CONCLUSIONS

Complex geometric structure and alignment of noncircular fibers in bundle affect the wicking action of hydrophobic polyester fiber assembly heavily. Capillary equivalent radius distribution, flux of saturated fiber bundle, capillary forming ability, and the instantaneous wicking velocity are discussed to acquire sequences for comprehensive comparison. Table VII presents four characteristic sequences qualifiedly. Shapes of S_{fen} and S_{cri} have much better integrative capillary effect for hydrophobic polyester bundle. Concave polygon shape is advantageous for surface driven flow in fiber bundle because of grooves. MFB and application software SG provide an efficient mathematical simulation and estimation method for liquid dynamic flowing in noncircular cross section fiber bundles.

References

1. Lukas, D.; Ning, P. Polym Compos 2003, 24, 314.
2. Dilip, R.; Arun, P. A.; Marchal, J. M. Text Res J 2001, 71, 813.
3. Ronald, P. R.; Peter, U.; Alex, L.; Lixin, X.; Daniel, B.; Russell, D.; Gordon, J. Compos A 1999, 30, 117.
4. Anne, P.; Mathilde, C.; Claude, C. Polym Test 2001, 20, 553.
5. Kamath, Y. K.; Hornby, S. B.; Weigmann, H. D.; Wilde, M. F. Text Res J 1994, 64, 33.
6. Amico, S.; Lekakou, C. Compos Sci Technol 2001, 61, 1945.

7. Hearle, J. W. S.; Grosberg, P.; Backer, S. Structural Mechanics of Fibers, Yarns, and Fabrics; Wiley-Interscience: New York, 1969.
8. Washburn, E. W. Phys Rev 1921, 57, 273.
9. Mohammad, P.; Martin, J. B. Phys Rev 2005, 71, 026301.
10. Mohammad, P.; Martin, J. B. Phys Rev 2005, 71, 026302.
11. Marcus, R. K.; Davis, W. C.; Knippel, B. C.; LaMotte, L.; Hill, T. A.; Perahia, D.; Jenkins, J. D. J Chromatogr A 2003, 986, 17.
12. Jakub, W.; Petra, D. Autex Res J 2003, 3, 64.
13. Brent, S.; Walter, H.; Brent, S.; Gerardo, M. J Sup Fluid 2000, 19, 87.
14. Lukas, D.; Soukupova, V.; Ning, P.; Parikh, D. V. Simulation 2004, 80, 547.
15. Lukas, D.; Glazyrina, E.; Ning, P. J Text Inst 1997, 88, 149.
16. Erik, K. Text Res J 1996, 66, 660.
17. McHale, G.; Newton, M. I. Colloid Surf A 2002, 206, 79.
18. Reed, C. M.; Wilson, N. J Phys D: Appl Phys 1993, 26, 1378.